AIP Journal of Applied Physics

Gettering of copper in silicon at half of the projected ion range induced by helium implantation

A. Peeva, P. F. P. Fichtner, D. L. da Silva, M. Behar, R. Koegler, and W. Skorupa

Citation: Journal of Applied Physics **91**, 69 (2002); doi: 10.1063/1.1418005
View online: http://dx.doi.org/10.1063/1.1418005
View Table of Contents: http://scitation.aip.org/content/aip/journal/jap/91/1?ver=pdfcov
Published by the AIP Publishing

Re-register for Table of Content Alerts

Create a profile.

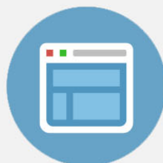

Sign up today!

[This article is copyrighted as indicated in the article. Reuse of AIP content is subject to the terms at: http://scitation.aip.org/termsconditions. Downloaded to] IP: 200.130.19.173 On: Thu, 20 Mar 2014 16:00:08

JOURNAL OF APPLIED PHYSICS VOLUME 91, NUMBER 1 1 JANUARY 2002

Gettering of copper in silicon at half of the projected ion range induced by helium implantation

A. Peeva[a)]
Forschungszentrum Rossendorf, POB 510119, D-01314 Dresden, Germany

P. F. P. Fichtner, D. L. da Silva, and M. Behar
UFRGS, POB 15051, 91501-970 Porto Alegre, Brazil

R. Koegler and W. Skorupa
Forschungszentrum Rossendorf, POB 510119, D-01314 Dresden, Germany

(Received 12 February 2001; accepted for publication 17 September 2001)

Secondary ion mass spectroscopy, transmission electron microscopy, Rutherford backscattering/channeling spectrometry, and elastic recoil detection analysis measurements were used to determine the Cu gettering behavior induced by He implanted into Si samples. This study was done in an iterative way by changing the implanted He fluence (5×10^{15}–$3\times10^{16}\,\mathrm{cm}^{-2}$), implantation temperature (room temperature or 350 °C), and implantation conditions (random or channel implants). Upon postimplantation annealing at 800 °C for 600 s, in addition to the gettering at the projected range (R_p) region, the room temperature implanted samples also present Cu gettering in a region corresponding to the half of the projected range ($R_p/2$) depth. Also a threshold fluence ($\Phi\approx7\times10^{15}\,\mathrm{at/cm^2}$) was determined for the appearance of the $R_p/2$ effect. In contrast, for the 350 °C implants, the Cu impurities are detected only close to the R_p region where the He induced cavities are formed. The gettering effect at $R_p/2$ region is discussed in terms of the cavity formation mechanisms and their influence on the point defect fluxes taking place during the thermal annealing.
© *2002 American Institute of Physics.* [DOI: 10.1063/1.1418005]

I. INTRODUCTION

Metal impurities can dramatically degrade the device properties in Si even when they are present at quite small concentrations below $10^{12}\,\mathrm{cm}^{-3}$.[1] High-energy ion implantation is being increasingly recognized as a promising method of achieving impurity gettering in Si. In the so-called "proximity gettering" technique a gettering layer is formed in the bulk of the Si wafer near the active device area by means of ion implantation and annealing.[2] The gettering layer collects unwanted metal impurities, thus reducing their concentration in the active device region. This process has been extensively studied in view of its potential application in advanced large scale integration technology.[3] The capture of metal impurities in MeV implanted Si has been detected by secondary ion mass spectrometry (SIMS) at the depth corresponding to the projected range, R_p, of the implanted ions, where a buried layer of extended lattice defects can be observed by transmission electron microscopy (TEM). However, in addition to the gettering at R_p, the trapping of metals at the $R_p/2$ region has also been detected for MeV ion implanted Si in the $10^{15}\,\mathrm{at/cm^2}$ fluence range, after thermal annealing in the 700–1000 °C temperature interval. This phenomenon, called "the $R_p/2$ gettering effect" was first observed by Tamura, Ando, and Ohya[4] by studying the gettering of O in czochralski (CZ) Si after MeV implantation of a variety of ions, such as C, F, Si, Ge, and As. The $R_p/2$ gettering effect is nowadays attributed to small vacancy-type defect clusters not visible in TEM images. The vacancy-rich region arises because of the slight displacement between the vacancy and interstitial generated in a high-energy knock on, as suggested by atomistic simulations.[5,6] The assumption of complete local point defect recombination (after the annealing) leads to a local vacancy excess at the near-surface region and an interstitial excess towards the R_P of the implant. The existence of defects at $R_P/2$ can be verified experimentally in most cases only by means of the impurity decoration method. Oxygen as well as the transition metals are very efficiently trapped in the $R_P/2$ region.[5–7] The supersaturation of vacancies can be monitored by the transient enhanced diffusion (TED) of Sb spikes. On the other hand, the TED of B in the same region indicates supersaturation of self-interstitials there.[8] The conventional variable-energy positron annihilation spectroscopy (PAS) was used to investigate the depth distribution of vacancy-type defects in the samples revealing metal gettering at $R_P/2$.[9–11] The data for the samples annealed at temperatures between 800 and 1000 °C (typical annealing temperatures in the $Rp/2$ effect studies) do not show the existence of vacancy-type defects. This means therefore, that the concentration of residual open volume defects is below the sensitivity of the PAS technique which was applied. However, other PAS investigations using low positron energies, combined with a stepwise removing of the surface in order to obtain high-resolution defect-depth profiling, shows the presence of open volume defects in the $R_P/2$ region.[11]

Irradiation of Si with light ions has also been studied for many years. In particular, He is known to agglomerate into

[a)]Author to whom correspondence should be addressed; electronic mail: peeva@fz.rossendorf.de

 © 2002 American Institute of Physics

[This article is copyrighted as indicated in the article. Reuse of AIP content is subject to the terms at: http://scitation.aip.org/termsconditions. Downloaded to] IP: 200.130.19.173 On: Thu, 20 Mar 2014 16:00:08

TABLE I. Depth of the $R_p/2$ and R_p peak positions and the cavity mean diameter for each implantation and annealing condition.

Anneal	Energy (keV)	Fluence (cm^{-2})	IT (°C)	Impl. Direction	Depth of $R_p/2$ peak position (μm)	Depth of R_p peak position (μm)	Cavity mean diameter (nm)
800 °C 10 min	40	TD	RT	Random		0.38	5 12
RTA (Ar)		LD	RT	Channeling	0.25	0.5	5 12.5
				Random	0.2	0.4	5.5 10.5
			HT	Channeling		0.45	4.5
				Random		0.35	4.5
		HD	RT	Channeling	0.25	0.45	6.5
				Random	0.2	0.35	5.5
			HT	Channeling		0.45	7
				Random		0.35	6
	20	LD	RT	Random	0.12	0.26	5.5 10
800 °C/1h FA (Ar)	40	LD	RT	Random		0.4	

cavities when implanted in Si.[12] Recently, great interest has developed toward the applications of these cavities in the Si technology. It has been demonstrated that He filled cavities act as powerful gettering centers of transition metals.[13–15] In particular, binding of Cu on the void internal surface has been intensively studied by Myers and Follstaedt.[13] Metals at low concentration are chemisorbed on the walls of the cavities. According to these authors, the binding energy for Cu on void internal surface is 2.22 eV. Moreover, Myers and Follstaedt[13] have also calculated the solution concentration after gettering of Cu by cavities. Cavity layers are able to reduce the impurity concentration by two orders of magnitude below the threshold for silicide precipitation. This is a result worth noting taking into consideration that the road map for silicon device fabrication[16] imposes levels for metal impurity concentration lower than the solid solubility which makes the metal gettering methods based on metal precipitation no longer usable.

In this work we extend the $R_p/2$-defect-related studies to the case of low defect production induced by the implantation conditions: light ion implanted at low energies in random or channel direction. Under this last condition the implantation damage is further reduced by almost one order of magnitude. Then, we present the results related to the $R_p/2$ effect observed in CZ-Si after He^+-ion implantation and annealing under a wide variety of experimental conditions. Namely: (a) random as well as channeling implantation into Si(100) channel direction; (b) different implantation conditions of fluence and energy; (c) high temperature (350 °C) or room temperature (RT) implantation and for a variety of annealing cycles and ways of introducing and redistributing the Cu into the samples.

Some results concerning 40 keV $He^{+\prime}$ $\phi = 0.8\times10^{16}$ He^+/cm^2 ion implantation into the channeling direction were previously published.[17] They are presently included for completeness.

II. EXPERIMENT

In the present experiment *n*-type (100) oriented CZ-Si wafers with a resistivity of 3–5 Ωcm were used. The samples were cleaned and etched to remove the native oxide and other impurities from the surface by using 10% HF acid. The implantations were performed using the 500 keV ion implantor of the IF-UFRGS. The random and channeling implantation were performed at 40 keV with $\phi = 0.8\times10^{16} He^+/cm^2$ [low dose (LD)] or 3.5×10^{16} He^+/cm^2 [high dose (HD)] at both: room temperature (RT) or at 350 °C [high temperature (HT)]. In random conditions two more RT experiments were performed: the first at 40 keV with $\phi = 0.5\times10^{16}$ at/cm^2 [threshold dose (TD)] and the second at 20 keV, with LD.

For the channeling implants the Si wafers were aligned using a 500 keV He beam with an angular divergence of the order of 0.03°. The samples were mounted on a three-axis goniometer with a precision of 0.005°. The backscattered particles were detected by a surface Si(Li) detector placed at 170° with respect to the beam direction. The overall resolution of the detecting system was about 13 keV. When the HT channel implants were performed we proceeded as follows. First the sample was RT aligned into Si(100) direction, then the goniometer was heated, and finally the alignment of the sample was checked again.

The implantation damage was annealed either by rapid thermal annealing (RTA) at 800 °C for 10 min or by furnace annealing (FA) at 800 °C for 1 h in an Ar ambient. All samples were contaminated with Cu by implantation at 20 keV, 1×10^{12} Cu^+/cm^2 on the backside of the Si wafers in order to study the gettering of Cu atoms at the defect layer. The redistribution of Cu throughout the sample bulk was done either simultaneously with the damage annealing or subsequently by implantation and redistribution of Cu using a second thermal treatment at 700 °C for 3 min. A summary of the implantation and annealing conditions is given in Table I.

The depth distribution of the equivalent of displaced silicon atoms was analyzed by Rutherford backscattering/channeling spectrometry (RBS/C) with a 1.2 MeV He^+ beam aligned to the (100) crystal direction. The distribution of the He content was investigated by elastic recoil detection analyses (ERDA) technique, using a 10 MeVC^{4+} beam. The samples were tilted 73.5° and the detector placed at 28° with

[This article is copyrighted as indicated in the article. Reuse of AIP content is subject to the terms at: http://scitation.aip.org/termsconditions. Downloaded to] IP: 200.130.19.173 On: Thu, 20 Mar 2014 16:00:08

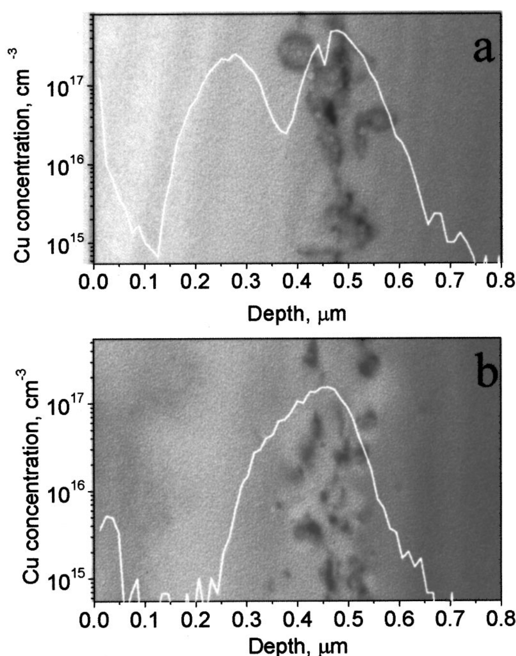

FIG. 1. (a) SIMS Cu depth profile for the sample implanted at 40 keV, 8×10^{15} He^+/cm^2, RT, channeling direction, contaminated by 1×10^{12} Cu^+/cm^2 after 800 °C/10 min RTA. The SIMS profile is combined with a XTEM bright field micrograph of the same sample. (b) The sample is the same as in (a) but implanted at HT.

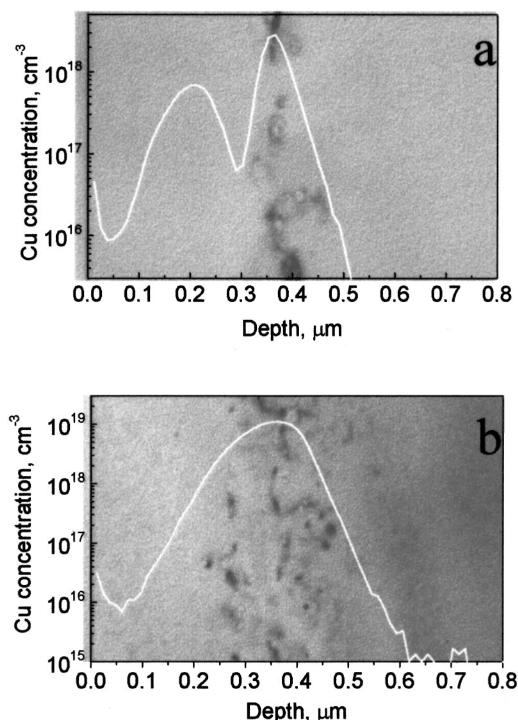

FIG. 2. (a) SIMS Cu depth profile for the sample implanted at 40 keV, 8×10^{15} He^+/cm^2, RT, random direction, contaminated by 1×10^{12} Cu^+/cm^2 after 800 °C/10 min RTA. The SIMS profile is combined with a XTEM bright field micrograph of the same sample. (b) The sample is the same as in (a) but implanted at HT.

respect to the beam direction. Transmission electron microscopy (TEM) analyses were applied at cross-sectioned and plan view samples using a Philips EM 300 microscope. The Cu distribution was measured by secondary ion mass spectrometry (SIMS).

III. RESULTS AND DISCUSSION

A. Low dose results

1. Channeling implantation

In order to reduce the implantation-induced damage in the $R_p/2$ region we performed channeling implantation into the $\langle 100 \rangle$ Si channel.

In Fig. 1(a) the Cu distributions are shown for the channel implantation performed at RT together with the corresponding cross-sectional transmission electron microscopy (XTEM) micrographs. The existence of two Cu peaks is clearly visible in the SIMS spectra in Fig. 1(a). The first one is located at ≅250 nm and the second one at ≈500 nm. The deeper peak is situated at the region of the He^+ projected range in agreement with the MARLOWE code predictions ($R_p = 510$ nm).[18] No evidence of Cu precipitation was observed. The Cu gettering in this region is consistent with what is known about the metal impurity gettering behavior of cavities in He^+ implanted Si.[19] The shallower Cu peak corresponds to the one described in the literature as the $R_p/2$ distribution.[4–7]

Figure 1(b) shows the Cu depth distribution for the 350 °C implant together with the corresponding XTEM micrograph. As can be clearly observed, the SIMS spectrum shows only one Cu peak with a maximum situated at ≈450 nm. This maximum is slightly shifted towards the surface as compared with the one obtained in the R_p region for the RT implant. This feature correlates with previous observations which demonstrate that under high temperature implantation the center of the He cavity layer is formed not at R_p but close to the maximum of the damage distribution induced by the ion implantation.[20]

A careful investigation of the TEM results reveals quite different microstructural features in both samples (Figs. 1(a) and 1(b)). After annealing, the RT He^+ implantation leads to a well-defined bimodal He cavity distribution, characterized by a population of large cavities with a mean diameter of 25 nm and a distribution of a smaller ones with a mean diameter of 10 nm. The depth position of the cavity layer correlates with the Cu peak at R_p in the corresponding SIMS profile. Our TEM investigations do not reveal the existence of any extended defect structure in the vicinity of the shallower Cu peak, which corresponds to the $R_p/2$ region. On the other hand, the HT He^+ implantation leads to a single mode He cavity distribution with a mean diameter of 9 nm. Both micrographs also show dislocation loops emerging from the cavity structures.

2. Random implantation

The Cu distribution for the RT random implant together with the corresponding XTEM micrograph are shown in Fig. 2(a). The existence of two Cu peaks is clearly indicated in the SIMS data. The first one is located at ≅200 nm and the second one at ≈370 nm. The deeper peak is situated at the region of the He^+ projected range as deduced from the

[This article is copyrighted as indicated in the article. Reuse of AIP content is subject to the terms at: http://scitation.aip.org/termsconditions. Downloaded to] IP: 200.130.19.173 On: Thu, 20 Mar 2014 16:00:08

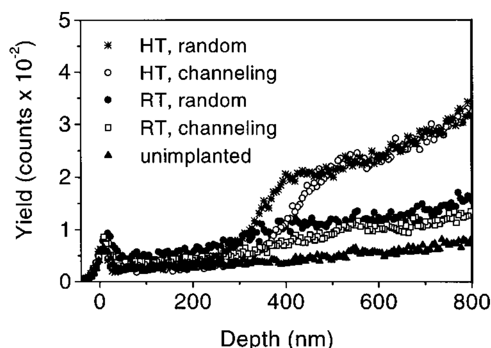

FIG. 3. RBS/C spectra from the samples implanted to the fluences of 8×10^{15} He^{+}/cm^{2} at RT channeling (open squares) and random (solid circles) direction compared with the same samples implanted at HT channeling (open circles) and random (stars) direction. The spectrum from an unimplanted sample (solid triangles) provides a scale for the minimum damage level detected in the RBS/C measurements

(TRIM) code range calculations ($R_p = 375$ nm).[21] As in the case of channeling implantation the shallower Cu peak can be ascribed as $R_p/2$ gettering peak.

Figure 2(b) shows the Cu depth distribution for the 350 °C implant together with the corresponding XTEM micrograph. In this case only one Cu peak situated at ≈350 nm can be observed. On the other hand, the TEM micrographs show a damage layer in the R_p region containing cavities and dislocations while no visible damage is observed at the $R_p/2$ region. These features agree with what was observed when the He was HT channel implanted.

3. RBS/C measurements for LD impants

The TEM observations can be compared with the results of the RBS/C measurements. The RBS/C spectra corresponding to the random RT (solid circles), random HT (stars), channeling RT (open squares), channeling HT (open circles) He implants before the thermal annealing, together with the spectrum corresponding to the nonimplanted sample (solid triangles) are shown in Fig. 3.

Comparing the RBS/C spectrum for the HT random implanted sample with the nonimplanted one it can be observed that up to a depth of ≈250 nm there is a small difference between both of them. For a depth above 250 nm the dechanneling yield of the spectra corresponding to the HT implant increases significantly. This feature is correlated with the nucleation and growth of the He cavities in the as-implanted sample, as revealed by TEM (not shown). On the other hand, the RBS/C spectrum corresponding to the random RT implant shows larger yield in the near-surface region as compared to the one corresponding to the nonimplanted sample. Near the surface the minimum channeling yield is $\chi_{\min} = 6\%$ (compared to the virgin sample, $\chi_{\min} = 4\%$) and goes up to $\chi_{\min} = 8\%$ at the R_p region. After performing the annealing, the RBS/C spectra of both RT and HT samples show in the $R_p/2$ region no difference when compared with the nonimplanted one.

The above measurements indicate that the HT implant does not induce any sizable damage in the $R_p/2$ region which is in agreement with the TEM observations. Concerning the RT implant the RBS/C measurements show that the implantation process leaves a damage that goes from the near surface up to the R_p region. The subsequent thermal treatment anneals out most of the damage in particular at the shallower region of the sample. This statement is supported by the TEM observations performed after the thermal anneal which show the existence of extended defects only at the R_p region.

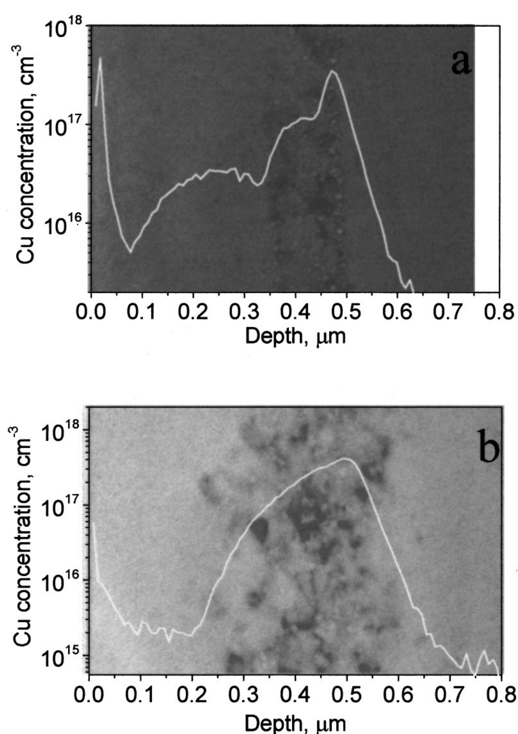

FIG. 4. (a) SIMS Cu depth profile for the sample implanted at 40 keV, 3.5×10^{16} He^{+}/cm^{2}, RT, channeling direction, contaminated by 1×10^{12} Cu^{+}/cm^{2} after 800 °C/10 min RTA. The SIMS profile is combined with a XTEM bright field micrograph of the same sample. (b) The sample is the same as in (a) but implanted at HT.

The results of the RBS/C measurements for the channeling implanted samples mirror the results obtained for the random implantation (Fig. 3). The only difference is that the obtained spectra are slightly shifted in depth by ≈100 nm as a consequence of the channeling implantation conditions. These results are in full agreement with the TEM observations.

B. High dose results

1. Channeling implantation

In Fig. 4 Cu distributions are shown for the implantation performed at RT (Fig. 4(a)) and 350 °C (Fig. 4(b)) together with the corresponding TEM micrographs. The SIMS profile obtained for the RT implant indicates the existence of one peak at 500 nm, a shoulder around 400 nm, and a broad Cu distribution centered at around 250 nm which can be characterized as a $R_p/2$ peak. Comparing Figs. 4(a) and 1(a), one can observe that the R_p peak in the present case is broader than the one obtained for the LD implant. It correlates with the cavity layer at R_p which for the HD [Fig. 4(a)] has much higher cavity concentration than for the LD [Fig. 1(a)]. For the HD implant the distribution of the cavities in the R_p

[This article is copyrighted as indicated in the article. Reuse of AIP content is subject to the terms at: http://scitation.aip.org/termsconditions. Downloaded to] IP: 200.130.19.173 On: Thu, 20 Mar 2014 16:00:08

region is inhomogeneous. Their concentration is higher at the deeper border of the defect layer. We suggest that this is the reason for the asymmetrical shape of the Cu profile at R_p in Fig. 4(a). No extended defects are observed in the vicinity of the $R_p/2$ peak as in the case of LD implantation [Fig. 1(a)].

On the other hand, the Cu depth profile obtained after the HT He implant shows the existence of only one peak that goes from 600 nm down to the 100 nm depth with the maximum around 400 nm. The TEM micrograph shows at the R_p region a buried defect layer containing dislocations and cavities with mean diameter about 15 nm slightly larger than the one for the RT temperature implant which is about 13 nm.

The RBS/C measurements in the as-implanted and annealed samples of the HT and RT implants indicate (not shown here) similar behavior to the one observed for the LD implants. Only in the case of the as-implanted RT sample the backscattering yield is slightly increased in the $R_p/2$ region ($\chi_{\min}=6\%$ for the as-implanted RT sample versus $\chi_{\min}=4\%$ for the unimplanted one). HT as-implanted and annealed samples do not show any measurable disorder at $R_p/2$.

2. Random implantation

Random implantations were performed, for both RT and HT conditions. The comparison of the TEM, SIMS, and RBS/C results of random and channeling implants shows similar characteristics. The random implants have the same features being present only shallower, about 100 nm compared to the channeling implantation spectra (not shown). The TEM analyses reveal cavities and dislocations located at R_P while no defects are observed in the $R_P/2$ region. The Cu SIMS profile consist of two peaks located around $R_P/2$ and R_P. The defect layer observed by TEM coincides with the deeper peak of the Cu SIMS profile. The depth positions of the Cu peaks measured by SIMS are given in Table I. The RBS/C measurements do not show any measurable disorder at $R_P/2$ in the HT as-implanted and in the annealed samples. Only the RT as-implanted sample reveals slightly higher backscattering yield in the $R_P/2$ region compared to the spectrum obtained from the virgin sample ($\chi_{\min}=6\%$ vs $\chi_{\min}=4\%$).

Comparing the Cu profiles of the results presented above one can see that the RT implants show a double peak structure for the LD and HD samples implanted at random or channeling direction. This feature can be deduced from the observation of Fig. 5. In the figure are displayed the Cu concentration depth profiles according to reduced depth (x/R_P) and concentration variables. The normalization has been achieved by scaling the concentration value and the depth position of the highest peak of each spectrum. On the other hand, when compared with LD and HD implants different features can be observed. The LD implanted sample shows two different Cu regions corresponding to R_p and $R_p/2$. At variance the Cu profile of the HD implant has three distinct regions: one in the R_p region corresponding to gettering on the larger cavities; a shoulder, which indicates gettering on the small bubbles, and a less pronounced peak corresponding to the $R_p/2$ region.

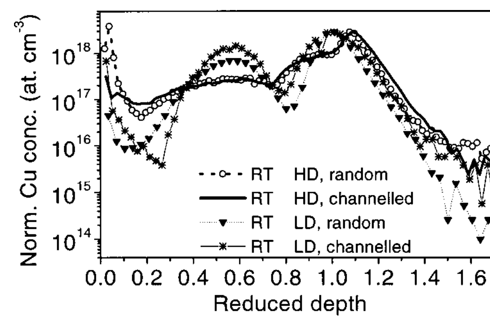

FIG. 5. Normalized SIMS Cu depth profiles vs the reduced depth of the RT implants: HD random (open circles), HD channeling (straight line), LD random (solid triangle), LD channeling (stars).

It is remarkable that all the HT implants display a single Cu peak located at R_p. This feature is seen in Fig. 6, which shows the normalized Cu concentration versus the reduced depth for both fluences and implantation directions. For all the HT implants a similar shape of the R_p gettering peak is observed.

3. ERDA results

We have performed ERDA measurements for all HD He^+-implanted samples. Here one example is presented and the similarities and the differences with all the implants are further discussed.

In Fig. 7 the ERDA spectra are displayed corresponding to the RT and HT implants in the as-implanted 7(a) and annealed state 7(b). The measured He concentration profiles for the as-implanted samples [Fig. 7(a)] show a different behavior for each implantation condition. The He concentration peak for the RT implanted sample is deeper as compared to the MARLOWE prediction. On the other hand, the HT implanted He distribution is located at the region where the MARLOWE code predict the maximum production of the implantation damage. The shift (≈50 nm) of the He concentration profile indicates that, depending on the implantation temperature, distinct cavity nucleation mechanism takes place. If the temperature of the sample during the implantation is high enough, then the He mobility is enhanced. The He vacancy reaction rate could be increased and the cavity formation takes place at the region of the maximum production of the damage.

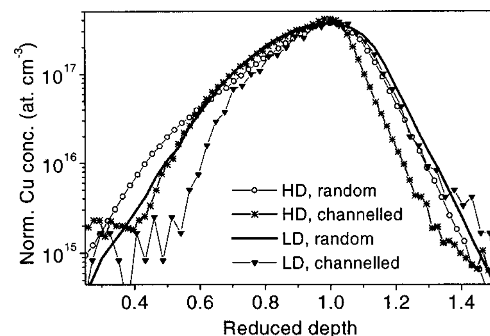

FIG. 6. Normalized SIMS Cu depth profiles vs the reduced depth of the HT implants: HD random (open circles), HD channeling (stars), LD random (straight line), LD channeling (solid triangles).

[This article is copyrighted as indicated in the article. Reuse of AIP content is subject to the terms at: http://scitation.aip.org/termsconditions. Downloaded to] IP: 200.130.19.173 On: Thu, 20 Mar 2014 16:00:08

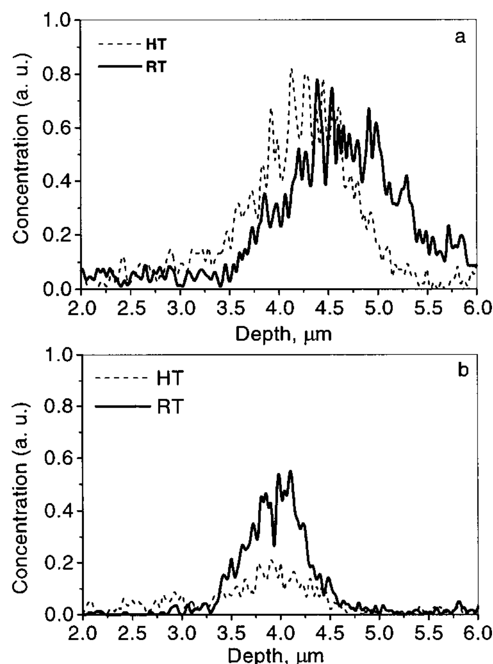

FIG. 7. (a) He concentration depth profiles from the as-implanted samples at 40 keV, $3.5\times10^{16}\,He^+/cm^2$, channeling direction at RT (straight line) and HT (dotted line) evaluated by ERDA; (b) the samples are the same as in (a) but annealed at 800 °C/10 min.

An inspection of the results after the annealing at 800 °C for 10 min [Fig. 7(b)] reveals that the RT implanted sample has lost about 80% of the He original as implanted content. On the other hand, the HT implanted sample lost about 90% of the He content. These values are in agreement with the results reported in Ref. 22. Both distributions become narrower and shift toward the surface. The maximum of the He concentration profile corresponds to the depth where the cavity layer is observed by means of TEM. The present results show that a measurable amount of He is still present within the cavity layer even after the 800 °C annealing.

The ERDA spectra of all the HD He channel implants show the same characteristics as described above. Only the channel He spectra is shifted toward the bulk. This agrees with the RBS/C measurements.

C. Threshold dose results

He^+ ions were implanted into Si at 40 keV with $\phi=0.5\times10^{16}\,at/cm^2$ at RT in random direction. In Fig. 8 the Cu distribution is shown together with the corresponding TEM micrograph. The Cu depth profile shows a single peak located in the R_p region with no indication of Cu trapping at the $R_p/2$ vicinity. This feature is interesting enough because it indicates a threshold fluence for the $R_p/2$ effect induced by He implantation. From the present results it can be concluded that this threshold fluence is between 0.5 and $0.8\times10^{16}\,at/cm^2$.

TEM observations of the sample in the as-implanted state (not shown here) indicate that after the He implantation there is no cavity formation. The last finding is in agreement with previously published results[18,19] where the authors report data on implantations done under the same conditions as the present ones: He^+ 40 keV $\phi=0.5\times10^{16}\,He^+/cm^2$. After annealing, the TEM observations indicate—see Fig. 8—the existence of a He induced cavity layer located at R_p. This result is at variance with previous published reports[23,24] where no cavities were found after furnace thermal annealing between 700 and 1000 °C. The authors of Refs. 18 and 19 assume that, if the cavities are not formed in the as-implanted sample, they cannot form during a subsequent high temperature annealing. However, we suggest that the annealing parameters (annealing ambient and the temperature ramp up) could be important for the formation of the He cavities. While RTA with a heating rate of about 20 °C/s under Ar ambient was performed in our study, furnace annealing in high vacuum was used by the abovementioned authors. Further experiments are needed to clarify the influence of the annealing on the He cavity nucleation and evolution.

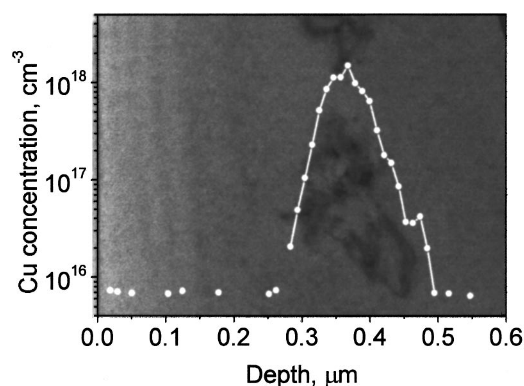

FIG. 8. SIMS Cu depth profile for the sample implanted at 40 keV, $5\times10^{15}\,He^+/cm^2$, RT, random direction, contaminated by $1\times10^{12}\,Cu^+/cm^2$ after 800 °C/10 min RTA. The SIMS profile is combined with a XTEM bright field micrograph of the same sample.

D. Lower energy results

Twenty keV He was implanted at RT in random direction with $\phi=0.8\times10^{16}\,at/cm^2$. In Fig. 9 the Cu distribution is shown together with the corresponding TEM micrograph. The SIMS measurements show the existence of two Cu

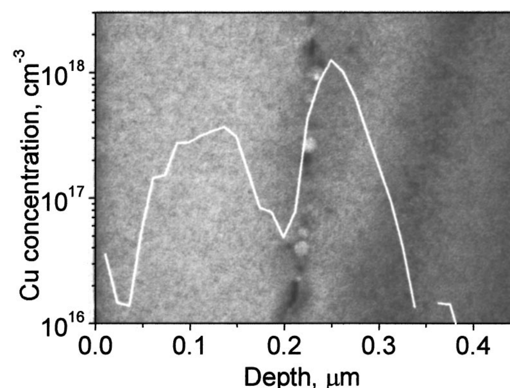

FIG. 9. SIMS Cu depth profile for the sample implanted at 20 keV, $8\times10^{15}\,He^+/cm^2$, RT, random direction, contaminated by $1\times10^{12}\,Cu^+/cm^2$ after 800 °C/10 min RTA. The SIMS profile is combined with a XTEM bright field micrograph of the same sample.

[This article is copyrighted as indicated in the article. Reuse of AIP content is subject to the terms at: http://scitation.aip.org/termsconditions. Downloaded to] IP: 200.130.19.173 On: Thu, 20 Mar 2014 16:00:08

peaks. The first is located at 240 nm, that is in the R_p region, and the second at about 120 nm, which corresponds to the $R_p/2$ vicinity. The TEM micrograph shows the existence of dislocations and cavities around the R_p region but no indication of extended defects in the $R_p/2$ region as for all results discussed above. The use of lower energy is a particular experiment to clear of the influence of the proximity of the surface to the defects at $R_p/2$. Experimental observations on the point defect diffusion show that both interstitials and vacancies exhibit migration interrupted by trapping at impurities (C, O) and dopant atoms.[25] The above study presents results showing the interstitials being faster than the vacancies. It is estimated that the trap-limited diffusion length of the vacancies in the CZ material (with O concentration $\sim 3 \times 10^{18}\,\mathrm{C\,m^{-2}}$) is $\sim 0.1\ \mu$m.[25] Hence it is expected that part of the excess vacancies in the $R_P/2$ region produced by the 20 keV implant could recombine either at the surface or with the excess interstitials in the R_P region (note that the distance between the $R_P/2$ gettering peak and the surface in Fig. 9 is $\sim 0.1\ \mu$m). The well pronounced double peak structure in the SIMS Cu profile observed for the 20 keV implant is similar to the one measured for 40 keV implant [Fig. 2(a)]. It can be concluded that no remarkable defect recombination at the surface is observed. This means that the proximity of the surface does not play a significant role for the appearance of the $R_p/2$ gettering effect in the frame of the used implantation and annealing conditions.

E. Additional experimental findings

(a) The $R_p/2$ effect of Cu in 40 keV He^+ RT implanted Si samples has not been observed for long annealing times, i.e., 1 h at 800 °C. In this case Cu gettering was found only at the R_p region (not shown). This means that the defects acting as gettering sites at $R_p/2$ have been removed during the prolonged annealing cycle.

(b) The Cu gettering has been found to be independent of the way of introducing Cu, simultaneously or subsequently to the damage annealing.

In Table I we have summarized all the results of the present experiment. There are quoted for each implantation and annealing conditions the peak positions of the corresponding Cu depth profile as obtained from SIMS experiments. In addition, we also show the characteristics of the damage, the region where it is located, as well as the mean size of the He cavities.

IV. MODELING

In the following section we will discuss the possible reasons for the appearance of the $R_p/2$ effect generated by He implants.

The appearance of a Cu peak in the $R_p/2$ region can be taken as an indication of the existence of small defect complexes acting as gettering centers for Cu. It is possible that these complexes or their precursors are formed by the implantation and are not removed by the RTA thermal process. From this point of view, the present results are quite similar to the previous ones, which have shown the $R_p/2$ effect induced by MeV implants. We will compare the defect production and recombination during ion implantation and subsequent annealing for the case of MeV implantation of heavier ions and for the case of keV implantation of He at random direction.

A. Predictions from ballistic models

For the MeV implantation of heavy ions, the $R_p/2$ gettering effect is attributed to the formation of excess vacancies at the $R_p/2$ region. According to binary collision calculations,[5,6,26,27] excess vacancies are formed because of the spatial separation of point defects due to the nonzero momentum component of the displaced Si atoms into the beam direction. In fact, the assumption of a complete local vacancy-interstitial annihilation during annealing leads to: (i) the formation of a vacancy-rich layer from the surface nearly up to R_p and (ii) the formation of an interstitial-rich region slightly extended beyond the R_p depth (with the maximum concentration of excess interstitials at about $1.2\,R_p$). In low-energy implants, these two regions are expected to react with each other to leave only excess interstitials but at higher energies, the effect of the vacancy-rich region is expected to be pronounced. One typical example for implantation conditions used in order to obtain $R_p/2$ effect in the high-energy implanted and annealed Si is 3.5 MeV self-ion implantation.[7,10,11] We will compare the excess vacancy production for this well investigated case with the low-energy implantations reported in this work. For 3.5 MeV Si^+ random implant into Si, TRIM/98 calculations provide a ratio of 0.182 excess vacancies per implanted Si^+ ion located within the surface and the R_p depth. The same calculations performed for 40 keV He^+ implant into Si result in an amount of 0.015 excess vacancies per implanted He^+ ion. Hence, the excess vacancy generation per implanted He^+ ion at the $R_p/2$ region is more than ten times lower than for the MeV Si^+ implant. However, it is important to note that the vacancy-rich region produced by the 3.5 MeV Si^+ ions extends from the surface to the depth $x_{\mathrm{Si}} \approx 2.25\ \mu$m. In contrast, the corresponding region for the 40 keV He^+ random implant extends from the surface to the depth $x_{\mathrm{He}} \approx 0.35\ \mu$m. As a consequence, the average number of excess vacancies for the Si and He cases are $\alpha_{\mathrm{Si}} = 8.1 \times 10^{-6}$ excess-vacancies/ion/Å and $\alpha_{\mathrm{He}} = 4.3 \times 10^{-6}$ excess-vacancies/ion/Å, which renders a ratio $\alpha_{\mathrm{He}}/\alpha_{\mathrm{Si}} \approx 0.5$. In addition, the corresponding excess vacancy ratio for the channel He implants is $\alpha^c_{\mathrm{He}}/\alpha_{\mathrm{Si}} \approx 0.1$. Considering the typical implanted fluences of $\phi_{\mathrm{Si}} \approx 0.5 \times 10^{16}\,\mathrm{cm^{-2}}$ and $\phi_{\mathrm{He}} \approx 0.8 \times 10^{16}\,\mathrm{cm^{-2}}$ one obtains a ratio for the effective excess vacancy concentration of $\alpha_{\mathrm{He}}\phi_{\mathrm{He}}/\alpha_{\mathrm{Si}}\phi_{\mathrm{Si}} \approx 0.8$ for the random implant case and of $\alpha^c_{\mathrm{He}}\phi_{\mathrm{He}}/\alpha_{\mathrm{Si}}\phi_{\mathrm{Si}} \approx 0.16$ for the channel one. However, for the fluence of $\phi_{\mathrm{He}} \approx 0.5 \times 10^{16}\,\mathrm{cm^{-2}}$ where no $R_p/2$ gettering appears (see Sec. III C), the estimated ratio is $\alpha_{\mathrm{He}}\phi_{\mathrm{He}}/\alpha_{\mathrm{Si}}\phi_{\mathrm{Si}} \approx 0.5$, a value well within the range where the $R_p/2$ effect is predicted according to the above reasoning. Hence, we are forced to conclude that the above ballistic arguments cannot provide a complete consistent explanation for the present observations of the $R_p/2$ gettering effect in He implanted Si.

[This article is copyrighted as indicated in the article. Reuse of AIP content is subject to the terms at: http://scitation.aip.org/termsconditions. Downloaded to] IP: 200.130.19.173 On: Thu, 20 Mar 2014 16:00:08

B. Processes which take place during annealing

Here is the point where one significant difference between the Si implant and the He implant must be taken into consideration: the defect structure in the R_p region after annealing. In the case of Si implantation the R_p region consists of extended defects (dislocation loops) with pure interstitial character. The excess silicon interstitials generated during the implantation process in this region plus the implanted ions themselves form these defects. Concerning the He implantation one has also to take into account the cavity formation and evolution. He atoms are known to be trapped by divacancies stabilizing them and favoring their evolution into more complex He–V clusters during annealing.[24,28] This results in accumulation and stabilization of vacancies in the R_p region contrary to what happens in the case of the Si implant. The silicon atoms displaced during the implantation diffuse during the annealing. They are trapped in the radiation damage close to the cavities and at the silicon surface. Recent studies report on the measurable recombination of the Si atoms at the surface after annealing at temperatures between 200 and 1200 °C.[24,29] The number of the silicon atoms trapped at the surface is slightly lower than the number of the vacancies trapped in the cavities.[19] This missing silicon atoms are supposed to form the dislocations around the cavities at R_p. It cannot be excluded that a part of the missing silicon atoms also contribute to the Cu gettering at $R_p/2$. On the other hand, small vacancy clusters not visible by TEM could also be gettering sides at $R_p/2$. Such small vacancy clusters can be stabilized by the He and be present in the samples even after annealing to the temperature as high as 850 °C.[30] Recently gettering of Au was also detected in the $R_p/2$ region of He implanted Si wafers.[31] This fact supports the idea of small vacancy clusters being the gettering sides at $R_p/2$.

The excess vacancy model discussed above predicts $1.5\times10^{14}\,\mathrm{cm}^{-2}$ excess vacancies in the $R_p/2$ region for the case of He implant to the fluence of $0.8\times10^{16}\,\mathrm{cm}^{-2}$. Using the TEM analyses we estimate that in this case the number of vacancies trapped in the cavities at R_p is $\approx2\times10^{15}\,\mathrm{cm}^{-2}$, a number which is one order of magnitude higher than the number of the calculated excess vacancies. Hence the equal number of displaced Si atoms was generated and not recombined with vacancies during the annealing. This means that local defect recombination is incomplete under our annealing conditions. Therefore, both types of small defect clusters, interstitial and vacancy type, potentially may exist at $R_p/2$ and are potential gettering centers for Cu. Further analyses will reveal which type of defects dominates the metal gettering.

The absence of Cu gettering at $R_p/2$ for the HT implantation is ascribed to the damage annealing that occurs during the implantation process. The high temperature enhances the local point defect recombination during implantation. From the plan view TEM analyses we have estimated the total cavity volume in terms of Si atoms displaced in order to open space for the cavity formation. We have estimated an amount of $\approx4\times10^{14}$ at./cm^2 for the case of 40 keV HT implant to the fluence of $1\times10^{16}\,\mathrm{He}^+/\mathrm{cm}^2$ [see Fig. 2(b)]. This value is five times lower than the one calculated for the corresponding RT implant [see Fig. 2(a)] for which the total cavity volume is $\approx2\times10^{15}\,\mathrm{cm}^{-2}$ (discussed above). This confirms the enhanced point defect recombination during implantation in the case of the HT implant which results in less nonrecombined vacancies trapped in the cavities and less nonrecombined interstitials may be present in the HT implanted samples compared with the RT implanted ones.

V. SUMMARY

In the present work we have shown that low-energy He implants in Si are able to induce Cu gettering at both the R_p and $R_p/2$ region during annealing at relatively high temperatures. The $R_p/2$ effect was found to be independent of the implantation conditions: random or ⟨100⟩ channeled one, but it strongly depends on the implantation temperature. Whenever He was implanted at RT, the $R_p/2$ effect was observed. However, HT implants led to the disappearance of the Cu peak in the $R_p/2$ region. This feature is attributed to damage recombination in the $R_p/2$ region during the implantation.

It was also found that a threshold He fluence ($0.6\times10^{16}<\phi\leqslant0.8\times10^{16}$ at/cm^2) is necessary for the appearance of a gettering layer at $R_p/2$. On the other hand, we have shown that the proximity of the surface does not play a significant role in the appearance of the $R_p/2$ gettering.

The He implantation induced $R_p/2$ effect was discussed on the basis of the radiation-induced defects, or in connection with the point defect fluxes associated with the formation of the He cavities. It was shown that the ballistic considerations alone cannot provide consistent predictions for the $R_p/2$ gettering effect at variance with the results obtained for medium-light ions ($6\leqslant Z_1\leqslant32$) MeV implanted into Si. In the present case, He leads to a different defect evolution during annealing compared to the case of MeV implantation of heavier ions. The appearance of the $R_p/2$ effect seems to depend either on the formation of He cavities, which trigger the absorption of vacancies and/or the emission of self-interstitial atoms from the R_p region, or on the stabilization of vacancy clusters at the $R_p/2$ region by the He atoms released from the cavities during the annealing processes. This assumption is also confirmed by the fact that RT channel or random implantation led to the $R_p/2$ effect irrespective of the different amount of damage that they cause at the $R_p/2$ region.

ACKNOWLEDGMENTS

The authors would like to acknowledge the financial support from the CAPES-DAAD (Brazilian-German) International Cooperation Program (PROBRAL). One of the authors, P. F. P. F, also acknowledges the support from the Alexander von Humboldt Foundation (Germany).

[1] T. E. Seidel, in *Materials Issues in Silicon Integrated Circuit Processing*, edited by M. Wittmer, J. Stimmell, and M. Strathman (Mater. Research Society Pittsburgh, 1986), p. 3.
[2] H. Wong, N. W. Cheung, P. K. Chu, J. Liu, and J. W. Mayer, Appl. Phys. Lett. **52**, 1023 (1988).
[3] J. L. Benton, P. A. Stolk, D. J. Eaglesham, D. C. Jacobson, J. Y. Chang, J.

[This article is copyrighted as indicated in the article. Reuse of AIP content is subject to the terms at: http://scitation.aip.org/termsconditions. Downloaded to] IP: 200.130.19.173 On: Thu, 20 Mar 2014 16:00:08

M. Poate, N. T. Há, T. E. Heynes, and S. M. Myers, J. Appl. Phys. **80**, 3275 (1996).
[4] M. Tamura, T. Ando, and K. Ohya, Nucl. Instrum. Methods Phys. Res. B **59/60**, 572 (1991).
[5] V. C. Venezia, D. J. Englesham, T. E. Haynes, A. Agarwal, D. C. Jacobson, H.-J. Gossmann, and F. H. Baumann, Appl. Phys. Lett. **73**, 2980 (1998).
[6] S. V. Koveshnikov and G. A. Rozgonyi, J. Appl. Phys. **84**, 3078 (1998).
[7] R. Koegler, D. Panknin, W. Skorupa, P. Werner, and A. B. Danilin, *Conference Proceedings of XI International Conference on Ion Implantation and Technology-96* (IEEE, Piscataway, NJ, 1996).
[8] D. J. Eaglesham, T. E. Haynes, H.-J. Gossmann, D. C. Jacobson, P. A. Stolk, and J. M. Poate, Appl. Phys. Lett. **70**, 3281 (1997).
[9] R. A. Brown, O. Kononchuk, A. Rozgony, S. Koveshnikov, A. P. Knights, P. J. Simpson, and F. Gonzalez, J. Appl. Phys. **84**, 2459 (1998).
[10] R. Kögler, A. Peeva, W. Anwand, G. Brauer, and W. Skorupa, Appl. Phys. Lett. **75**, 1279 (1999).
[11] R. Krause-Rehberg, F. Börner, and F. Redmann, Appl. Phys. Lett. **77**, 3932 (2000); S. M. Myers, H. J. Stein, and D. M. Follstaedt, Phys. Rev. B **51**, 9742 (1995).
[12] M. Myers, H. J. Stein, and D. M. Follstaedt, Phys. Rev. B **51**, 9742 (1995).
[13] S. M. Myers and D. M. Follstaedt, J. Appl. Phys. **79**, 1337 (1996).
[14] V. Raineri, Solid State Phenom. **57,58**, 43 (1997).
[15] J. Wong-Leung, C. E. Ascheron, M. Petravic, R. G. Elliman, and J. S. Williams, Appl. Phys. Lett. **66**, 1231 (1995).
[16] *The National Roadmap for Semiconductors* (Semiconductor Industry Association, San Jose, CA, 1997).
[17] P. F. P. Fichtner, M. Behar, J. R. Kaschny, A. Peeva, R. Koegler, and W. Skorupa, Appl. Phys. Lett. **77**, 972 (2000).
[18] M. T. Robinson, Nucl. Instrum. Methods Phys. Res. B **48**, 408 (1990).
[19] S. M. Myers, D. M. Bishop, D. M. Follstaedt, H. J. Stein, and W. R. Wampler, Mater. Res. Soc. Symp. Proc. **283**, 549 (1993).
[20] P. F. P. Fichtner, A. Peeva, M. Behar, G. de M. Azevedo, R. L. Maltez, R. Koegler, and W. Skorupa, Nucl. Instrum. Methods Phys. Res. B **161–163**, 1038 (2000).
[21] J. B. Biersack and L. G. Haggmark, Nucl. Instrum. Methods Phys. Res. B **174**, 257 (1980).
[22] J. R. Kaschny, P. F. P. Fichtner, A. Muecklich, U. Kreissig, R. A. Yankov, R. Koegler, A. B. Danilin, and W. Skorupa, Mater. Res. Soc. Symp. Proc. **469**, 451 (1997).
[23] V. Raineri, P. G. Fallica, G. Percolla, A. Battaglia, M. Barbagallo, and S. U. Campisano, J. Appl. Phys. **78**, 3727 (1995).
[24] V. Raineri, M. Saggion, and E. Rimini, J. Mater. Res. **15**, 1449 (2000).
[25] E. Rimini, S. Coffa, S. Libertino, G. Mannino, F. Priolo, and V. Privitera, Defect Diffus. Forum **153–155**, 137 (1998).
[26] K.-H. Heinig and H.-U. Jaeger. Proceedings of the 1st ENDEASD Workshop, Santorini/Greece, April, 1999, p. 297 (unpublished).
[27] O. W. Holland, L. Xie, B. Nielsen, and D. S. Zhou, J. Electron. Mater. **25**, 99 (1996).
[28] S. Estreicher, J. Weber, A. Derecskei-Kovacs, and D. Marynick, Phys. Rev. B **55**, 5037 (1997).
[29] W. Fukarek and J. Kaschny, J. Appl. Phys. **86**, 4160 (1999).
[30] R. Brusa, G. Karwasz, N. Tiengo, A. Zecca, F. Corni, R. Tonini, and G. Ottaviani, Phys. Rev. B **61**, 10154 (2000).
[31] R. Kalyanaraman (private communications).

[This article is copyrighted as indicated in the article. Reuse of AIP content is subject to the terms at: http://scitation.aip.org/termsconditions. Downloaded to] IP: 200.130.19.173 On: Thu, 20 Mar 2014 16:00:08